MODELLING AND ANALYSIS OF MECHANICAL SYSTEMS DYNAMICS

A technique of experiment aided virtual prototyping to obtain the best spindle speed during face milling of large-size structures

Krzysztof J. Kalinski · **Marek A. Galewski** · **Michal R. Mazur** ·
Natalia Morawska

Abstract The paper presents an original method concerning vibration suppression problem during milling of large-size and geometrically complicated workpieces with the use of novel way of selecting the spindle speed. This consists in repetitive simulations of the cutting process for subsequent values of the spindle speed, until the best vibration state of the workpiece is reached. An appropriate method of obtaining a computational model, called a modal approach, consists in identifying the parameters of the workpiece model created using the Finite Element Method (FEM). Thanks to the results of the identification of the modal subsystem obtained by the Experimental Modal Analysis (EMA) method, it can be stated that the parameters obtained from the experiment and delivered from the computational model have been correctly determined and constitute reliable process data for the simulation tests. The Root Mean Square (RMS) values of time domain displacements are evaluated. The efficiency of the proposed approach is evidenced by chosen technique of mechatronic design, called Experiment Aided Virtual Prototyping (EAVP). The proposed method is verified on the basis of the results of the experimental research of the relevant milling process.

K. J. Kalinski · M. A. Galewski · M. R. Mazur ·
N. Morawska (✉)
Faculty of Mechanical Engineering, Gdansk University of
Technology, G. Narutowicza 11/12, 80-233 Gdansk,
Poland
e-mail: natalia.morawska@pg.edu.pl

1 Introduction

Tool-workpiece relative vibrations are the main reason of various problems occurring during a process of machining of large-size structures [1]. Some examples of these problems are reduction of the quality of the machined surface, reduction of overall machine tool productivity, increased tool wear and, in extreme cases, even the destruction of a tool or a workpiece [2]. Regeneration phenomenon, the kinematic excitation caused by repetitious immersion of cutting edges into the workpiece and the internal feedback interactions in the machine-holder-workpiece-tool system are recognized as the most important causes of vibration during milling, especially *chatter* vibration [3–5]. There are many vibration suppression and avoidance techniques developed over the years [3, 6] however, many of them have been applied for research purposes only. In industrial practice, in order to avoid vibration, "safe" parameters (e.g. small depths of cutting, low feed and tool rotation speeds) for milling process have to be selected. Moreover, because of a lack of ability of making a lot of "material" experiments during production process, methods of searching for the

required technology ought to be effective. Although many of the proposed approaches usually avoid *chatter* vibration, vibrations caused by other causes, such as an unbalanced tool or workpiece flexibility, are still present. The machining process efficiency is often limited as well. In order to increase efficiency while retaining surface quality and minimizing vibration level, including *chatter* avoidance, the method of spindle speed selection with the use of Experiment Aided Virtual Prototyping (EAVP) is proposed. This method is developed based on experience from the previous authors' works [7–9]. It belongs to the wider group of vibration reduction methods that utilize spindle speed variation [10, 11], or matching the spindle speed to the selected properties of the machining process and the workpiece [12–14]. The advantage of these methods is that they generally need neither modifications of the machine tool structure nor utilization of sophisticated equipment, like for example: active damping methods [15–19], semiactive methods [20, 21] or dynamic feedforward control applied towards heavy machine tools [22].

The methodology of vibration suppression through spindle speed variation met a lot of successful applications. For example, one way to reduce vibration level during both roughing and finishing industrial operations is to determine the optimal spindle speed [4, 7, 23, 24]. Moreover, the approach reflects its convenience in practical use, because of necessary interference only with technological parameters; all conditions of the workpiece fixing remain unchangeable. A promising previous method of vibration reduction could be based on adjusting constant spindle speed to the optimal phase shift angle between subsequent tool passes [12]. The same results were obtained by the authors on a basis of the assumption, that the whole work of instantaneous cutting forces along accompanying cutting layer thickness has to be minimized [7, 23]. Taking into account the influence of the dynamic properties of the workpiece on the amplitude and frequency of vibration implies the need to create a "map" determining the optimal spindle speeds at various points of the workpiece surface clamped on the machine tool [8, 9], in accordance with the condition of minimum work of the cutting forces. However, the above approach concerns flexible workpieces having small dimensions. In case of large workpieces, the so called basic optimal spindle speed map does not meet the assumed requirements and is

only the first approximation; the best spindle speed should be sought under dynamic conditions of the milling process. The other important drawback is that the approach considers only natural frequencies accompanying the identified poles of the system but omits the more important and intensive influence of harmonic frequencies of the excited vibrations. The latter means that due to more complicated nature of the large-size milling process vibration it cannot be tied only to the *chatter* phenomenon.

A dedicated solution described in the paper is the proposed original technique of the Experiment Aided Virtual Prototyping (EAVP). Determination of favorable states of vibration on a basis of reliable calculation models during large-size milling processes is a principal indication for solving the subjective task [25, 26].
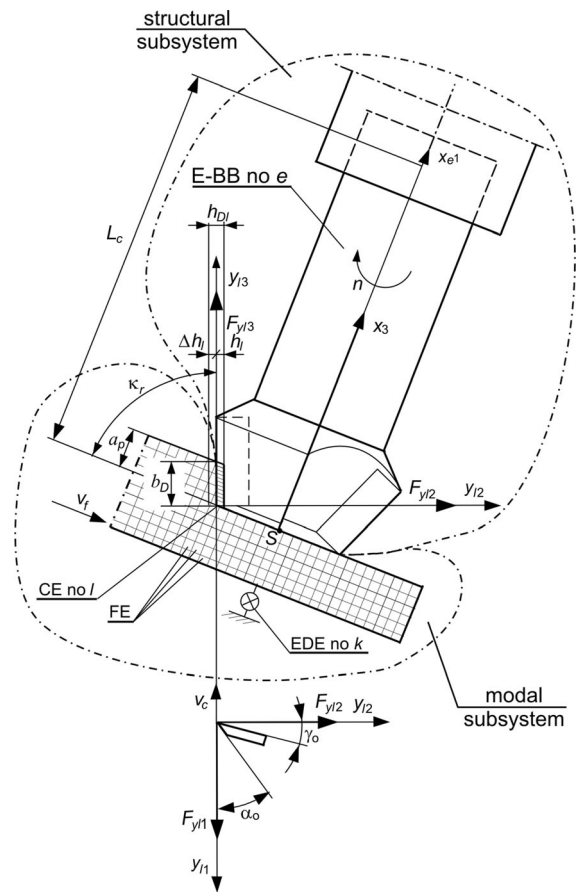
The paper was the result of a thorough reorganization and significant extension of the material presented in [27]. It is organized as follows. After the introduction containing a description of various methods of vibration reduction in machine tools, a model for computer simulation is proposed, with particular emphasis on cutting dynamics and description in hybrid coordinates. Then the original method of selecting the best spindle speed using the full FEM model of the workpiece and modal analysis is presented. The next part shows the results of simulation and experimental research on milling selected surfaces of a large-size object. The elaboration ends with conclusions and a list of contemporary bibliography.

2 Simulation model

2.1 Cutting process dynamics

Dynamic analysis of a face milling process of a flexible workpiece (Fig. 1) has been performed, based on the following assumptions [23, 28].

- The spindle, together with the tool fixed in the holder, and the table with the workpiece, are separated from the machine tool structure. The remaining parts of the milling machine are recognized as ones whose influence can be neglected [4, 7, 29].

Fig. 1 Scheme of a face milling of a flexible workpiece

- Flexibility of the tool and flexibility of the workpiece are considered. The latter especially concerns a large-size flexible workpiece [30].
- Coupling Elements (CEs) are applied for modeling the cutting process dynamic interaction [23, 28]. It is a phenomenological model taking into account the properties of the processed material, as well as the relationship between the instantaneous values of the components of cutting forces and the geometry of the cutting layer. Modeling using CE well reflects the physical nature of the material being processed.
- An effect of first pass of the edge along cutting layer causes proportional feedback, and the effect of multiple passes causes delayed feedback additionally. The latter makes it possible to include the multiple regenerative effect in the calculation model, which is one of the potential causes of loss of tool-workpiece vibrations stability.

For instantaneous contact point between the chosen tool edge and the workpiece (idealized by CE no. l), proportional model of the cutting dynamics is included [23, 28]. Based on this model, the cutting forces depend proportionally on the instant thickness of the cutting layer $h_l(t)$, as well as on the instant width of the cutting layer $b_l(t)$; both differ in time. According to the direction of the action, we separate cutting force component F_{yl1} acting along nominal cutting velocity v_c, cutting force component F_{yl2} acting along cutting layer thickness, and additionally in contrast to previous approaches [23, 31]—cutting force component F_{yl3} acting along cutting layer width (Fig. 1). The individual components of the cutting force are described by the following equations:

$$F_{yl1}(t) = \begin{cases} k_{dl}b_l(t)h_l(t), & h_l(t) > 0 \wedge b_l(t) > 0, \\ 0, & h_l(t) \leq 0 \vee b_l(t) \leq 0, \end{cases}$$
(1)

$$F_{yl2}(t) = \begin{cases} \mu_{l2}k_{dl}b_l(t)h_l(t), & h_l(t) > 0 \wedge b_l(t) > 0, \\ 0, & h_l(t) \leq 0 \vee b_l(t) \leq 0, \end{cases}$$
(2)

$$F_{yl3}(t) = \begin{cases} \mu_{l3}k_{dl}b_l(t)h_l(t), & h_l(t) > 0 \wedge b_l(t) > 0, \\ 0, & h_l(t) \leq 0 \vee b_l(t) \leq 0, \end{cases}$$
(3)

where

$$b_l(t) = b_D(t) - \Delta b_l(t),$$
$$h_l(t) = h_{Dl}(t) - \Delta h_l(t) + \Delta h_l(t - \tau_l),$$

$b_D(t)$—desired cutting layer width, $b_D(t) = a_p(t)/\cos \kappa_r$, $\Delta b_l(t)$—dynamic change in cutting layer width for CE no. l, $h_{Dl}(t)$—desired cutting layer thickness for CE no. l, $h_{Dl}(t) \cong f_z \cos\varphi_l(t)$, $\Delta h_l(.)$—dynamic change in cutting layer thickness for CE no. l, k_{dl}—average dynamic specific cutting pressure for CE no. l, μ_{l2}, μ_{l3}—cutting force ratios for CE no. l, as quotients of forces F_{yl2} and F_{yl1}, and forces F_{yl3} and F_{yl1}, τ_l—time-delay between the same position of CE no. l and of CE no. $l-1$, $a_p(t)$—desired depth of cutting, κ_r—edge angle, f_z—feed per edge, $\varphi_l(t)$—angular position of CE no. l [10].

Zero cutting forces in Eqs. (1)—(3) correspond to the loss of contact between the cutting tool edge and the workpiece, which causes the first effect of nonlinearity of the model, due to the limitation of the cutting force characteristics. As a result, these

equations describing cutting forces for CE no. l in the case of such a three-dimensional model can be represented in matrix notation:

$$\underbrace{\begin{Bmatrix} F_{yl1} \\ F_{yl2} \\ F_{yl3} \end{Bmatrix}}_{\breve{\mathbf{F}}_l(t)} = \underbrace{\begin{bmatrix} k_{dl}b_D(t)h_{Dl}(t) \\ \mu_{l2}k_{dl}b_D(t)h_{Dl}(t) \\ \mu_{l3}k_{dl}b_D(t)h_{Dl}(t) \end{bmatrix}}_{\breve{\mathbf{F}}_l^{\,0}(t)}$$

$$-\left\{ \underbrace{\begin{bmatrix} 0 & k_{dl}b_D(t) & k_{dl}h_{Dl}(t) \\ 0 & \mu_{l2}k_{dl}b_D(t) & \mu_{l2}k_{dl}h_{Dl}(t) \\ 0 & \mu_{l3}k_{dl}b_D(t) & \mu_{l3}k_{dl}h_{Dl}(t) \end{bmatrix}}_{\breve{\mathbf{D}}_{Pl}^{(l)}(t)} - \underbrace{\begin{bmatrix} 0 & k_{dl}\Delta b_l(t) & 0 \\ 0 & \mu_{l2}k_{dl}\Delta b_l(t) & 0 \\ 0 & \mu_{l3}k_{dl}\Delta b_l(t) & 0 \end{bmatrix}}_{\breve{\mathbf{D}}_{Pl}^{(n)}(t)} \right\}$$

$$\cdot \underbrace{\begin{Bmatrix} q_{zl}(t) \\ \Delta h_l(t) \\ \Delta b_l(t) \end{Bmatrix}}_{\Delta\breve{\mathbf{w}}_l(t)} + \left\{ \underbrace{\begin{bmatrix} 0 & k_{dl}b_D(t) & 0 \\ 0 & \mu_{l2}k_{dl}b_D(t) & 0 \\ 0 & \mu_{l3}k_{dl}b_D(t) & 0 \end{bmatrix}}_{\breve{\mathbf{D}}_{Ol}^{(l)}(t)} - \underbrace{\begin{bmatrix} 0 & k_{dl}\Delta b_l(t) & 0 \\ 0 & \mu_{l2}k_{dl}\Delta b_l(t) & 0 \\ 0 & \mu_{l3}k_{dl}\Delta b_l(t) & 0 \end{bmatrix}}_{\breve{\mathbf{D}}_{Ol}^{(n)}(t)} \right\}$$

$$\cdot \underbrace{\begin{Bmatrix} q_{zl}(t-\tau_l) \\ \Delta h_l(t-\tau_l) \\ \Delta b_l(t-\tau_l) \end{Bmatrix}}_{\Delta\breve{\mathbf{w}}_l(t-\tau_l)} \tag{4}$$

or using the abbreviated notation:

$$\breve{\mathbf{F}}_l(t) = \breve{\mathbf{F}}_l^{\,0}(t) - \left(\breve{\mathbf{D}}_{Pl}^{(l)}(t) - \breve{\mathbf{D}}_{Pl}^{(n)}(t) \right)\Delta\breve{\mathbf{w}}_l(t)$$
$$+ \left(\breve{\mathbf{D}}_{Ol}^{(l)}(t) - \breve{\mathbf{D}}_{Ol}^{(n)}(t) \right)\Delta\breve{\mathbf{w}}_l(t-\tau_l), \tag{5}$$

where $\breve{\mathbf{F}}_l(t)$—vector of cutting forces of CE no. l, $\breve{\mathbf{F}}_l^{\,0}(t)$—vector of cutting forces of CE no. l, resulted from a desired cutting geometry and kinematics, $\breve{\mathbf{D}}_{Pl}^{(l)}(t)$—matrix of linear proportional feedback interactions, $\breve{\mathbf{D}}_{Pl}^{(n)}(t)$—matrix of non-linear proportional

feedback interactions, $\breve{\mathbf{D}}_{Ol}^{(l)}(t)$—matrix of linear time-delayed feedback interactions, $\breve{\mathbf{D}}_{Ol}^{(n)}(t)$—matrix of non-linear time-delayed feedback interactions, $\Delta\breve{\mathbf{w}}_l(t)$—vector of deflections of CE no. l at instant of time t, $\Delta\breve{\mathbf{w}}_l(t-\tau_l)$—vector of deflections of CE no. l at instant of time $t-\tau_l$, $q_{zl}(t)$—relative displacement of edge and workpiece along direction y_{l1} at instant of time t, $q_{zl}(t-\tau_l)$—relative displacement of edge and workpiece along direction y_{l1} at instant of time $t-\tau_l$.

The second effect of the non-linearity of the model is the geometric non-linearity resulting from the dependence of the matrix $\breve{\mathbf{D}}_{Pl}^{(n)}(t)$ and $\breve{\mathbf{D}}_{Ol}^{(n)}(t)$ on the

dynamic change in the width of the cutting layer $\Delta b_l(t)$.

Vector (5) can also be described in six-dimensional space, i.e.,:

$$\begin{aligned} \mathbf{F}_l(t) = \mathbf{F}_l^0(t) &- \left(\mathbf{D}_{Pl}^{(l)}(t) - \mathbf{D}_{Pl}^{(n)}(t)\right)\Delta\mathbf{w}_l(t) \\ &+ \left(\mathbf{D}_{Ol}^{(l)}(t) - \mathbf{D}_{Ol}^{(n)}(t)\right)\Delta\mathbf{w}_l(t - \tau_l), \end{aligned} \quad (6)$$

where:

$$\mathbf{F}_l(t) = col\left(\breve{\mathbf{F}}_l(t), \mathbf{0}_{3\times 1}\right), \quad (7)$$

$$\Delta\mathbf{w}_l(t) = col\left(\Delta\breve{\mathbf{w}}_l(t), \mathbf{0}_{3\times 1}\right), \quad (8)$$

$$\mathbf{F}_l^0(t) = col\left(\breve{\mathbf{F}}_l^0(t), \mathbf{0}_{3\times 1}\right), \quad (9)$$

$$\mathbf{D}_{Pl}^{(l)}(t) = \begin{bmatrix} \breve{\mathbf{D}}_{Pl}^{(l)}(t) & \mathbf{0} \\ \mathbf{0} & \mathbf{0} \end{bmatrix}_{6\times 6}, \quad (10)$$

$$\mathbf{D}_{Pl}^{(n)}(t) = \begin{bmatrix} \breve{\mathbf{D}}_{Pl}^{(n)}(t) & \mathbf{0} \\ \mathbf{0} & \mathbf{0} \end{bmatrix}_{6\times 6}, \quad (11)$$

$$\mathbf{D}_{Ol}^{(l)}(t) = \begin{bmatrix} \breve{\mathbf{D}}_{Ol}^{(l)}(t) & \mathbf{0} \\ \mathbf{0} & \mathbf{0} \end{bmatrix}_{6\times 6}, \quad (12)$$

$$\mathbf{D}_{Ol}^{(n)}(t) = \begin{bmatrix} \breve{\mathbf{D}}_{Ol}^{(n)}(t) & \mathbf{0} \\ \mathbf{0} & \mathbf{0} \end{bmatrix}_{6\times 6}. \quad (13)$$

The above considerations exemplify a significant progress with respect to the previous ones [7, 31], because now the non-linear feedback interactions are additionally included.

In order to simplify further notation, relationship (6) takes the form:

$$\mathbf{F}_l(t) = \mathbf{F}_l^0(t) - \mathbf{D}_{Pl}(t)\Delta\mathbf{w}_l(t) + \mathbf{D}_{Ol}(t)\Delta\mathbf{w}_l(t - \tau_l), \quad (14)$$

where:

$$\mathbf{D}_{Pl}(t) = \mathbf{D}_{Pl}^{(l)}(t) - \mathbf{D}_{Pl}^{(n)}(t), \quad (15)$$

$$\mathbf{D}_{Ol}(t) = \mathbf{D}_{Ol}^{(l)}(t) - \mathbf{D}_{Ol}^{(n)}(t). \quad (16)$$

As a result of a milling process modeling, a hybrid system, which consists of the separated subsystems, is obtained (Fig. 1). These subsystems are:

- modal subsystem, i.e., a stationary model of the Finite Element Method (FEM) of a flexible workpiece supported by Elastic-Damping Elements (EDE), which moves at the desired feed speed v_f. At first, the subsystem is idealized as a set of tetragonal 10-node Finite Elements (FE) [7, 23] and has a large number of degrees of freedom. However, after modal transformation [7, 23], the behavior of this subsystem is described by a vector of its modal coordinates **a**, whose number is in practice much smaller than the corresponding number of degrees of freedom. Therefore, when we consider a finite number of subsystem normal modes *mod*, we define its dynamic properties using:

  $\boldsymbol{\Omega} = diag(\omega_{0i})$—matrix of natural angular frequencies of the modal subsystem; $i = 1, \ldots, mod$. This is also called the *stiffness modal matrix*;
  $\boldsymbol{\Psi} = [\boldsymbol{\Psi}_1 \quad \ldots \quad \boldsymbol{\Psi}_{mod}]$—matrix of considered mass-normalised normal modes of the modal subsystem; $i = 1, \ldots, mod$;
  $\mathbf{Z} = diag(\zeta_i)$—matrix of dimensionless damping coefficients (also called *modal damping*) of the modal subsystem; $i = 1, \ldots, mod$;

- structural subsystem, i.e., a non-stationary discrete model of a rotating milling cutter with a given spindle speed n (i.e., a flexible finite element as Euler–Bernoulli Bar (E-BB) no. e [7, 23] having a local coordinate system x_{e1}, x_{e2}, x_{e3}) and the cutting process (i.e., Coupling Element (CE) no l [23, 28] placed in the momentary position of the "active" cutting edge [23]). The cutting edges are "active" when they come into contact with the workpiece and the others are called "inactive". The subsystem's behavior is described by a vector of its generalized coordinates **q**. The dynamic properties of the decoupled structural subsystem (i.e., the E-BB modeling the tool itself) are determined by the matrices of inertia **M**, damping **L** and stiffness **K**;

- abstractive connecting subsystem as a conventional contact point S between tool and workpiece. Its generalized coordinates are related to other coordinates using time-dependent constraints equations [23, 24]. The latter allows us to eliminate these generalized coordinates from the description of the behavior of the hybrid system.

2.2 Dynamics of flexible details in hybrid system coordinates

Vector of deflections of CE no. l is expressed as a function of vector of generalized coordinates $\mathbf{q}$ and vector of modal coordinates $\mathbf{a}$. Hence the following relationship is obtained [7, 23]:

$$\Delta \mathbf{w}_l(t) = \mathbf{T}_l(t)\mathbf{q} - \mathbf{W}_l(t)\mathbf{a} = [\mathbf{T}_l(t) \quad -\mathbf{W}_l(t)] \left\{ \begin{array}{c} \mathbf{q} \\ \mathbf{a} \end{array} \right\}$$
$$= [\mathbf{T}_l(t) \quad -\mathbf{W}_l(t)]\underbrace{\boldsymbol{\xi}}_{\boldsymbol{\xi}} \tag{17}$$

where: $\boldsymbol{\xi} = \left\{ \begin{array}{c} \mathbf{q} \\ \mathbf{a} \end{array} \right\}$—vector of hybrid coordinates of the hybrid system, $\mathbf{T}_l(t)$—transformation matrix of

$$\left[\begin{array}{c} \mathbf{T}_l^T(t) \\ -\mathbf{W}_l^T(t) \end{array} \right] \mathbf{F}_l(t) = \left[\begin{array}{c} \mathbf{T}_l^T(t) \\ -\mathbf{W}_l^T(t) \end{array} \right] \mathbf{F}_l^0(t)$$
$$- \left[\begin{array}{cc} \mathbf{T}_l^T(t)\mathbf{D}_{Pl}(t)\mathbf{T}_l(t) & -\mathbf{T}_l^T(t)\mathbf{D}_{Pl}(t)\mathbf{W}_l(t) \\ -\mathbf{W}_l^T\mathbf{D}_{Pl}(t)\mathbf{T}_l(t) & \mathbf{W}_l^T(t)\mathbf{D}_{Pl}(t)\mathbf{W}_l(t) \end{array} \right] \left\{ \begin{array}{c} \mathbf{q}_s \\ \mathbf{a}_m \end{array} \right\}$$
$$+ \left[\begin{array}{c} \mathbf{T}_l^T(t)\mathbf{D}_{Ol}(t) \\ -\mathbf{W}_l^T(t)\mathbf{D}_{Ol}(t) \end{array} \right] \Delta \mathbf{w}_l(t - \tau_l). \tag{18}$$

As the result of the hybrid system's consideration, the matrix equation of dynamics of non-stationary model of the milling process in hybrid coordinates will have the following form [7, 23, 24]:
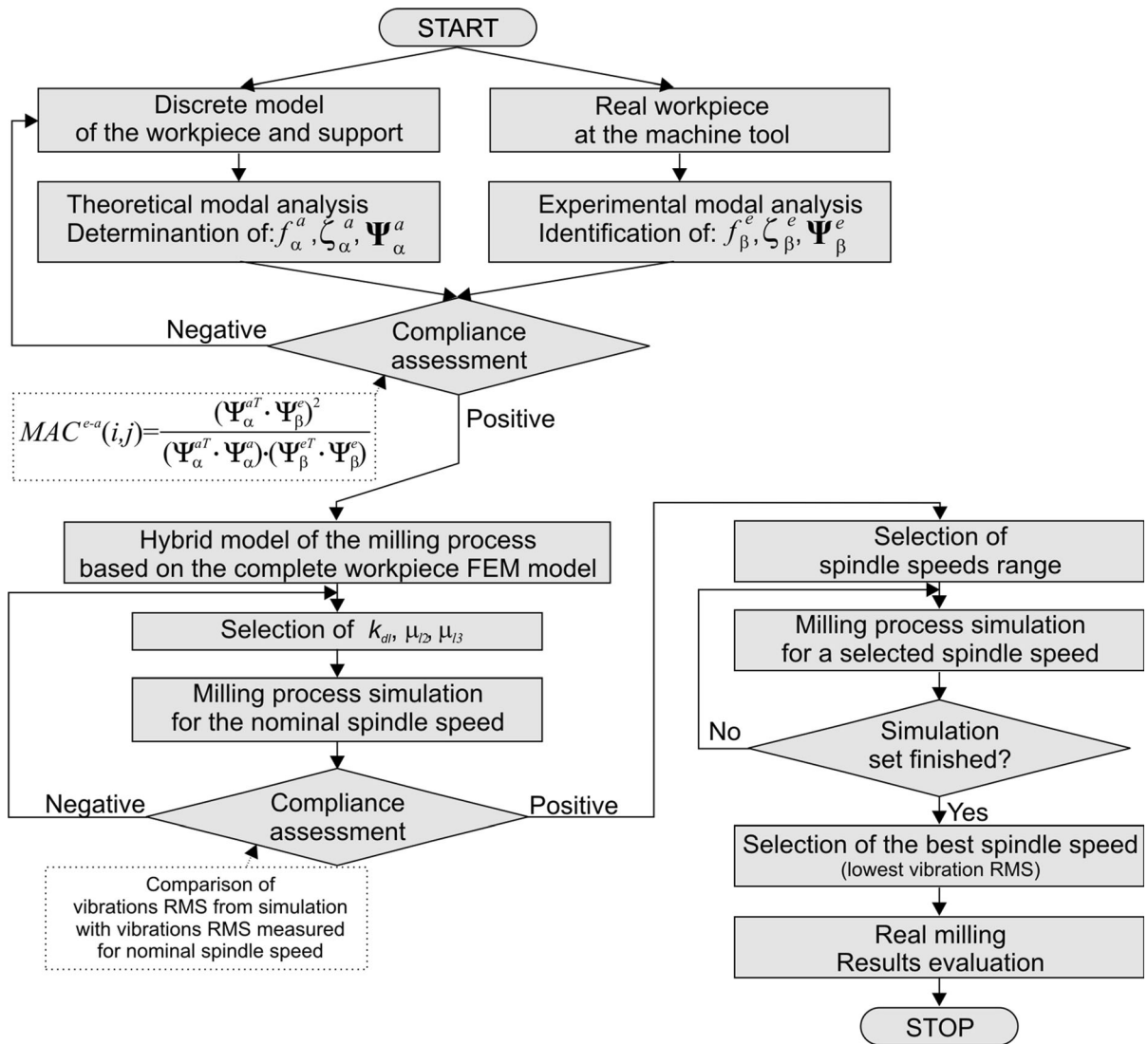
$$\left[\begin{array}{cc} \mathbf{M} & \mathbf{0} \\ \mathbf{0} & \mathbf{I} \end{array} \right] \ddot{\boldsymbol{\xi}} + \left[\begin{array}{cc} \mathbf{L} & \mathbf{0} \\ \mathbf{0} & 2\mathbf{Z}\boldsymbol{\Omega} \end{array} \right] \dot{\boldsymbol{\xi}}$$
$$+ \left[\begin{array}{cc} \mathbf{K} + \sum_{l=1}^{i_l} \mathbf{T}_l^T(t)\mathbf{D}_{Pl}(t)\mathbf{T}_l(t) & -\sum_{l=1}^{i_l} \mathbf{T}_l^T(t)\mathbf{D}_{Pl}(t)\mathbf{W}_l(t) \\ -\sum_{l=1}^{i_l} \mathbf{W}_l^T(t)\mathbf{D}_{Pl}(t)\mathbf{T}_l(t) & \boldsymbol{\Omega}^2 + \sum_{l=1}^{i_l} \mathbf{W}_l^T(t)\mathbf{D}_{Pl}(t)\mathbf{W}_l(t) \end{array} \right] \boldsymbol{\xi}$$
$$= \left[\begin{array}{c} \sum_{l=1}^{i_l} \mathbf{T}_l^T(t)\mathbf{F}_l^0(t) + \mathbf{T}_l^T(t)\mathbf{D}_{Ol}(t)\Delta \mathbf{w}(t - \tau_l) \\ -\sum_{l=1}^{i_l} \mathbf{W}_l^T(t)\mathbf{F}_l^0(t) - \mathbf{W}_l^T(t)\mathbf{D}_{Ol}(t)\Delta \mathbf{w}(t - \tau_l) \end{array} \right], \tag{19}$$

displacements' vector $\mathbf{q}$ from coordinate system x_{e1}, x_{e2}, x_{e3} of E-BB no. e, to coordinate system y_{l1}, y_{l2}, y_{l3} of CE no. l [23, 28, 31], $\mathbf{W}_l(t)$—matrix of constraints between displacements' vector in modal coordinates $\mathbf{a}$, and displacements in coordinate system y_{l1}, y_{l2}, y_{l3} of CE no. l [23, 31].

After transformation of the vector of force interaction of CE no. l (Eq. 14) to hybrid coordinates, we obtain:

where i_l—number of „active" coupling elements [23, 28].

Simulations in the time domain, based on Eq. (19), take into account the most important non-linear effects observed in real milling operations, i.e., the relative vibration of the tool and the workpiece along the thickness and width of the cutting layer, loss of contact

Fig. 2 Scheme of the EAVP on a basis of the modal approach

of the cutting edge with the workpiece, multiple regenerative effect, through successive change of the geometrical position of the momentary connection of the tool with the workpiece. In this way they demonstrate the advantages of performing time simulations instead of the traditional linear stability analysis.

In order to identify the modal model of the flexible workpiece [which is part of Eq. (19)], the matrix of normal modes Ψ and the matrix of corresponding natural angular frequencies Ω of the modal subsystem must be determined. The separation of the modal subsystem from the entire non-stationary structure

allows us to reduce the finite element model to several modes, the number of which depends on the importance and the need to select modes for further analysis. As a result, the size of the model is significantly reduced.

Normal modes are unchanged over time because it is assumed that the modal subsystem remains stationary during the cutting process. For this reason, normal modes Ψ and angular frequencies Ω can be identified by:

- computer software for calculating eigenfrequencies and corresponding normal modes of discretely

idealized systems. In practice, high-degree-of-freedom calculation models, created using the Finite Element Method (FEM), are applied;

- Experimental Modal Analysis (EMA) methods. For example, impact modal tests are performed on the workpiece actually installed on the machine tool's table.
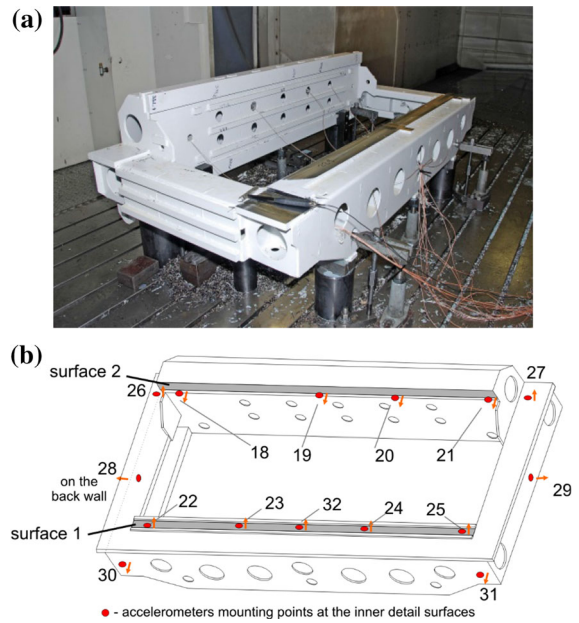
Both approaches are recommended due to the need for mutual verification of the results obtained.

The number of modal coordinates is generally much lower than the number of generalized FEM coordinates, therefore calculations should be performed much more efficiently. The dominant vibration modes can be different at different places of the manufactured surface, especially for workpieces of large size and complicated shapes. Therefore, in the case of a modal model computed analytically using the FEM model, it is usually most convenient to use the set of the first few elastic modes. It is assumed that the lower order modes are more important in terms of quality and quantitative properties of the cutting process simulation. However, in the case of the modal model obtained directly from the experiment, it is assumed that the modes identified on the basis of the Frequency Response Function (FRF) measured only at driving points lying on the manufactured surface dominate.

3 Selection of the best spindle speed based on simulation of cutting process and full FEM model of the workpiece

In the proposed technique of Experiment Aided Virtual Prototyping, based on the modal approach, the following procedure of spindle speed selection is suggested (Fig. 2).

1. Creation of the FEM model of flexible workpiece including its support modelled as a set of Elastic-Damping Elements (EDEs), and computation of normal modes.
2. Modal parameters' estimation with the use of the EMA techniques.
3. Verification of the FEM model using the Modal Assurance Criterion (MAC) [32].

(a)

(b)

Fig. 3 Test workpiece: **a** clamped on the machine table, **b** simplified scheme of the workpiece with indicated mounting points for accelerometers

$$MAC^{e-a}(\alpha, \beta) = \frac{\left(\mathbf{\Psi}_\alpha^{aT} \cdot \mathbf{\Psi}_\beta^e\right)^2}{\left(\mathbf{\Psi}_\alpha^{aT} \cdot \mathbf{\Psi}_\alpha^a\right) \cdot \left(\mathbf{\Psi}_\beta^{eT} \cdot \mathbf{\Psi}_\beta^e\right)},$$
(20)

where $\mathbf{\Psi}_\alpha^a$—vector of normal mode no. α calculated from the FEM model, $\mathbf{\Psi}_\beta^e$—vector of normal mode no. β identified by modal tests.

4. Once the FEM model of the whole workpiece is assumed to be valid, dominant normal modes are selected in order to be used in modal subsystem of the hybrid model of the milling process.
5. Determination of cutting process simulation parameters (k_{dl}, μ_{l2}, μ_{l3}) by conforming milling simulations performed for nominal (standard) spindle speed of the process to the results of real cutting performed for the same speed. Obtaining the above compliance condition is based on a comparison of the Root Mean Square (RMS) values of tool-workpiece relative displacements, obtained from simulation and the implementation of the cutting process.
6. Simulations of the milling process for various spindle speeds from the selected range. Cutting process parameters determined in p. 5, are applied.

7. For a desired set of the simulated milling processes, vibration levels are observed (for example, the RMS value of tool-workpiece relative displacements), and as the result, the best spindle speed is selected.
8. Real milling with the best spindle speed selected.

The advantage of this method is that the exact model of the entire workpiece and supports is used for simulation. This can be especially important in the case of complicated part geometry. On the other hand, however, using the full model allows us to specify all normal modes that are necessary to model the dynamic behavior of the entire workpiece. It may include modes that are not really relevant to modeling machined surface behavior. This can unnecessarily complicate the model and thus extend the simulation time.

An important feature of the developed method based on EAVP technique, from the point of view of prospective industrial applications, is that in order to select the best spindle speed, the required "material" experiments of the actual process were carried out only twice, i.e., for standard process parameters and improved.

4 Simulation and experimental results

4.1 The workpiece

The experimental research concerned investigating the dynamic behavior of a large workpiece (total size $2061 \times 1116 \times 540$ mm) made of STW22 03M steel (Fig. 3a) and clamped on a table of the MIKROMAT 20 V portal milling center. The workpiece was selected from the common production program of one cooperating industrial company. For a purpose of the research the following measurement equipment setup was applied [33]: 15 DJB A/120 V accelerometers with measurement range $\pm$ 75 g; PCB 086C03 modal hammer, range $\pm$ 2224 N; National Instruments PXI-8106 controller with NI PXI 4496 24-bit simultaneous DAQ card working under the LabView 2016 RT environment. All signals were sampled with frequency at least 5 kHz (during cutting experiments) or 15 kHz (during modal tests). Measurements were performed using custom developed software.

There were two surfaces milled (Fig. 3b). For surface 1, full face milling was performed first by the tool moving from the left (i.e., starting from a vicinity of accelerometer 22) to the right. Down milling was performed next by the tool moving in the opposite direction (i.e., starting from a vicinity of accelerometer 25). These two passes formed one complete operation. Length of the surface was 1778 mm, and width—57.5 mm. The milling was performed by the 4-edge Sandvik face milling cutter R390-044C4-11M060, ϕ44 mm, cutting edge angle $\kappa = 90°$. For surface 2 only one pass of down milling was performed by the tool moving from the left (i.e., starting from a vicinity of accelerometer 18). Length of the surface was 1789 mm, width—55 mm. Milling was performed by the 11-edge Sandvik face milling cutter R390-125Q40-17H, ϕ125 mm, cutting edge angle $\kappa = 90°$. The use of tools with cutting edge angles $\kappa = 90°$ does not require taking into account in the calculation model the phenomenon of tooling system bending, typical for relatively large cutter diameters [34].

The measuring points were selected in such a way as to be able to record measuring signals mainly along the milled surfaces. Due to the limited number of accelerometers in experimental research, there were 9 of them, i.e. 5 on the first surface and 4 on the second, placed at equal intervals, and the remaining—in other less important places of the workpiece (Fig. 3b).

4.2 Standard parameters

The standard parameters used for milling process in the common production scheme of cooperating industry, in case of the presented workpiece were:

- for surface $1 - n = 1300$ rev/min, $v_f = 600$ mm/min, $a_p = 1$ mm;
- for surface $2 - n = 560$ rev/min, $v_f = 1233$ mm/min, $a_p = 1$ mm.

The vibration level during milling with the above mentioned parameters is treated as a reference to compare the results of the method used to search for the best spindle speed. It is worth noting that the vibrations during milling with standard parameters were generally very low, so further reduction of vibrations was a significant challenge of the research.

Meccanica

Table 1 Natural frequencies and MAC values for identified (EMA) and computed (FEM) normal modes
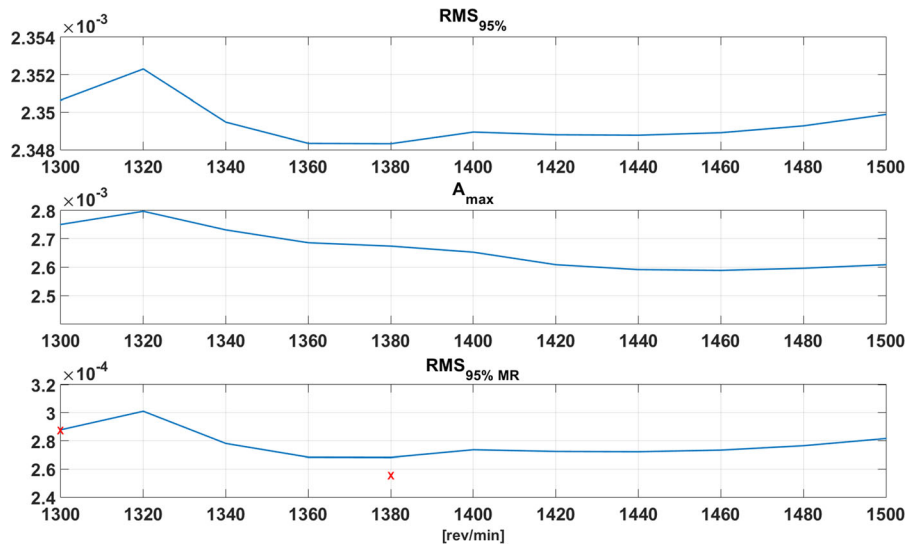
Mode no.	EMA identification (ERA)		FEM (PERMAS + MEDINA software)		*MAC*
	Frequency (Hz)	Modal damping (%)	Frequency (Hz)	Modal damping (%)	
1	91.2	10.19	**90.3123**	10.19	0.96
2	111.2	5.92	110.978	*5.92*	–
3			151.18	*2.0*	–
4	151.3	4.21	**153.184**	4.21	0.95
	170.9	6.30			–
5			196.85	*2.02*	–
	216.1	4.36			–
6	234.5	2.05	**235.861**	2.05	0.98
	253.3	0.84			–
7	266.7	1.63	**263.49**	1.63	0.95
8	279.4	1.62	**286.333**	1.62	0.82
9	313.6	1.63	**312.817**	1.63	0.92
10	307.1	1.61	**331.486**	1.61	0.82
	342.0	1.21			–
11	377.8	1.35	**373.387**	1.35	0.89
	396.0	1.48			–
12			409.794	*1.48*	–
13			426.212	*1.48*	–
14	452.0	2.02	**468.307**	2.02	0.96
15			497.005	*0.5*	–

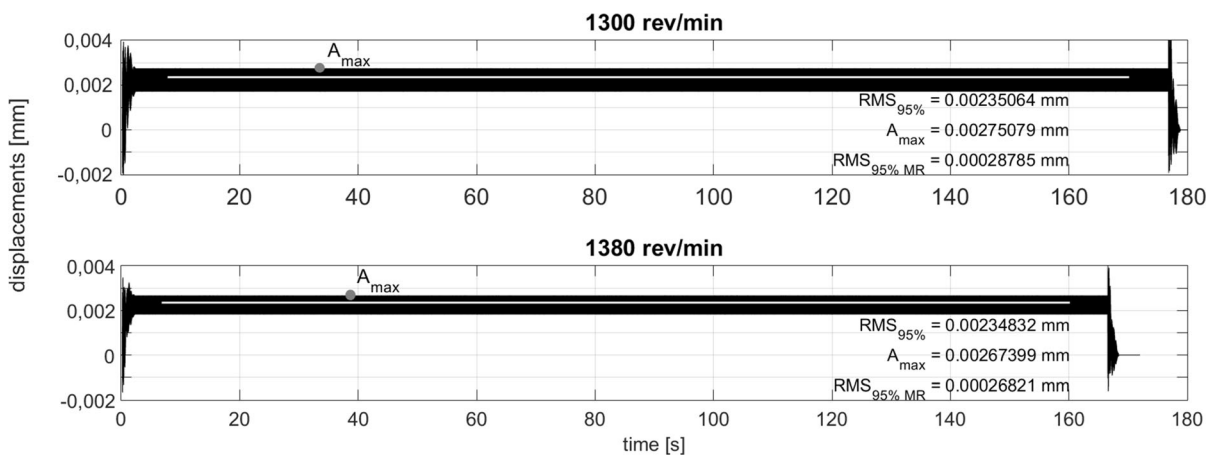### 4.3 Modal identification and spindle speed selection

The experimental modal tests of the workpiece were performed. 15 global modes were identified with the use of Eigenvalue Realisation Algorithm (ERA) [23, 35]. The FEM model of the workpiece and its support was tuned to correlate it with the identified modes. With the use of appropriate FEM software i.e., PERMAS and MEDINA [23], calculation model of the workpiece, composed of 12 511 156 nodes, 7 764 895 10-node tetragonal finite elements, 2158 bar elements (RBAR) and 423 rigid bodies (RBE), was obtained. 15 natural frequencies and accompanying normal modes of the workpiece mounted in the supports were calculated. 9 of the modes identified by the ERA conformed with modes calculated by the FEM (MAC values are over 0.8 and the corresponding computed frequencies are in bold, see Table 1). For these modes modal damping coefficients were selected in accordance with the identification results. For the rest of the modes, damping coefficients were

estimated (italic letters in Table 1). Approximate time to obtain the expected compatibility of the modal model of the workpiece using a laptop computer equipped with an Intel® Core ™ i7-6700HQ CPU 2.60 GHz processor and having RAM 32 GB, was about 240 min. The vectors of mass-normalized normal modes for points lying on the machined surface were then exported to the original AMIKRO4 cutting process simulation software running in the 64-bit MSYS2 MinGW environment on the same type of portable computer. Simulations were performed for a set of the defined spindle speeds using FEM model based on 15 modes having modal parameters as are shown in columns 4 and 5 (Table 1). The above means that both the FEM model and the modal models were constructed and then subjected to experimental validation in the real range of interesting frequencies of 500 Hz.

Subsequent step of the modal procedure of searching for the best spindle speed using EAVP when milling large-size workpieces (Fig. 2) is to create non-stationary calculation model of the face milling
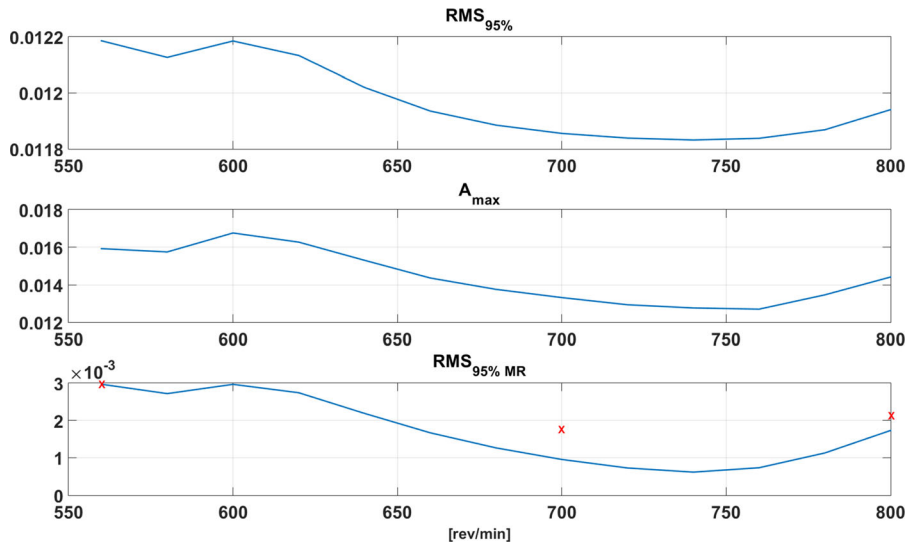
Fig. 4 Modal approach for full milling of workpiece, surface 1, indices values with respect to the simulated spindle speed, x—average results of measurements (see, Table 3)

Fig. 5 Modal approach, simulation results for 1300 and 1380 rev/min, surface 1

process of the indicated surfaces. The reason is that a compliance ought to be obtained between the RMS values of simulated vibrations' displacements and the measured ones during standard production conditions. Of course, one can also consider using other quantities to validate milling process simulation models. However, it should be noted that the simulated models are non-stationary and strongly non-linear. Therefore, other conformity assessment measures, based e.g. on the frequency analysis of steady vibration states, do not apply here. RMS is the best measure for assessing displacements in the examined issue.

The corresponding RMS values of simulated plots, adjusted to milling at standard parameters (see p. 4.2) were: for full milling of surface 1—0.000287 mm, for down milling of surface 2—0.002971 mm. As a result of the selection, the following parameters of the hybrid model are adapted to milling simulations to meet the RMS values compliance condition: for surface 1, k_{dl}= 500 daN/mm^2, $\mu_{l2} = 0.4$, $\mu_{l3} = 0.42$; and for surface 2, k_{dl}= 500 daN/mm^2, $\mu_{l2} = 0.4$, $\mu_{l3} = 0.24$. The approximate time of determining values of these parameters was: for surface 1—5 min., for surface 2—4 min.

Springer

Fig. 6 Modal approach for down milling of workpiece, surface 2, indices values with respect to the simulated spindle speed, x—average results of measurements (see, Table 3)

Table 2 Selected spindle and feed speeds

Speed selection	a_p (mm)	Spindle speed n (rev/min)					Feed speed v_f (mm/min)				
		A22	A23	A32	A24	A25	A22	A23	A32	A24	A25
Workpiece, surface 1											
Standard	1	1300					600				
Modal	1	1380					637				
		A18	A19	A20		A21	A18	A19	A20		A21
Workpiece, surface 2											
Standard	1	560					1233				
Modal	1	700		800			1541		1761		

The speed range was 1300…1500 rev/min for surface 1, and 550…800 rev/min for surface 2. The lower limit is the standard spindle speed used for milling the selected workpiece, and the upper limit is the maximum allowable speed for the selected tool and the maximum cutting speed for the insert. Spindle speeds below 1300 and 550 rev/min were not simulated as the intention of the performed research was not only to reduce vibration level but also to increase process efficiency. For every spindle speed, vibration level was observed and three indices were calculated, i.e.,:

- $RMS_{95\%}$—RMS of tool-workpiece relative displacements calculated for 95% of the whole cutting time. The remaining 5% consist of transient effects of the tool entrance and exit out of the workpiece;
- A_{max}—maximum amplitude of tool-workpiece relative displacements calculated for the same period as for $RMS_{95\%}$;
- $RMS_{95\%MR}$—RMS of tool-workpiece relative displacements calculated for 95% of the whole cutting time (similarly to $RMS_{95\%}$), but relatively to the mean value of the considered vibrations (MR—mean related). Thus, this indicator is equivalent to standard deviation of vibrations. This can be

Table 3 RMS values of displacements of performed milling operations for measurement points on the milled surfaces

Milling type	Speed selection	Displacements RMS (mm)					
		A22	A23	A32	A24	A25	Average
Workpiece, surface 1							
Full	Standard	0.000128	0.000340	0.000432	0.000390	0.000144	0.000287
Down	Standard	0.000275	0.001376	0.001581	0.001281	0.000261	0.000955
Full	Modal	0.000174	**0.000232**	**0.000320**	**0.000305**	0.000203	**0.000247**
Down	Modal	0.000298	**0.000500**	**0.000671**	**0.000584**	0.000327	**0.000476**
		A18	A19	A20	A21		Average
Workpiece, surface 2							
Down	Standard	0.003524	0.002460	0.002310	0.002556		0.002992
							0.002433
Down	Modal	**0.001913**	**0.001546**	0.002486	**0.001708**		**0.001730**
							0.002097

Bold values indicate better results

Table 4 Relative change of RMS values of displacements of performed milling operations for measurement points on the milled surfaces

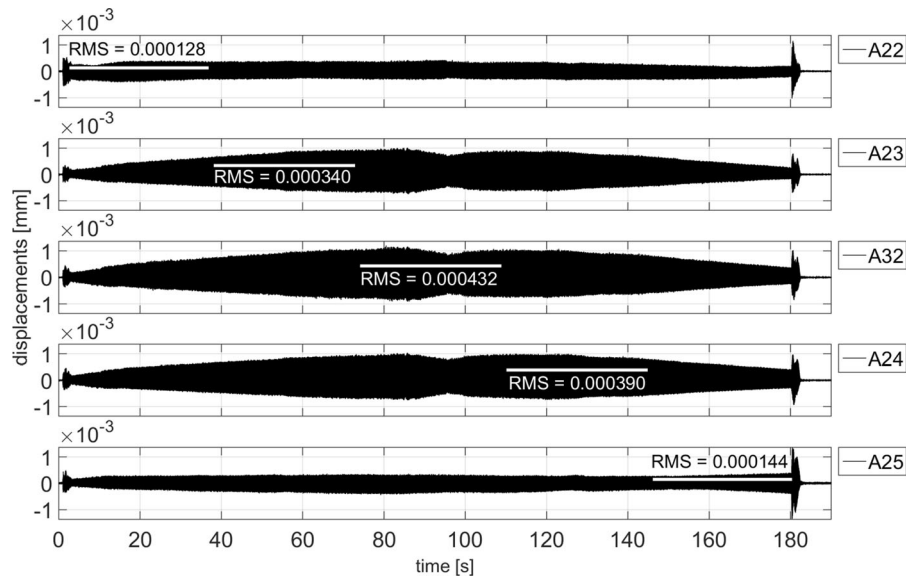| Milling type	Speed selection	Change in RMS values (%)					
		A22	A23	A32	A24	A25	Average
Workpiece, surface 1							
Full	Standard	–	–	–	–	–	–
Down	Standard	–	–	–	–	–	–
Full	Modal	35.9	− 31.8	− 25.9	− 21.8	41.0	− 13.9
Down	Modal	8.4	− 63.7	− 57.6	− 54.4	25.3	− 50.1
		A18	A19	A20	A21		Average
Workpiece, surface 2							
Down	Standard	–	–	–	–		–
							–
Down	Modal	− 45.7	− 37.2	7.6	− 33.2.		− 42.2
							− 13.8

Milling with standard spindle speed taken as the reference

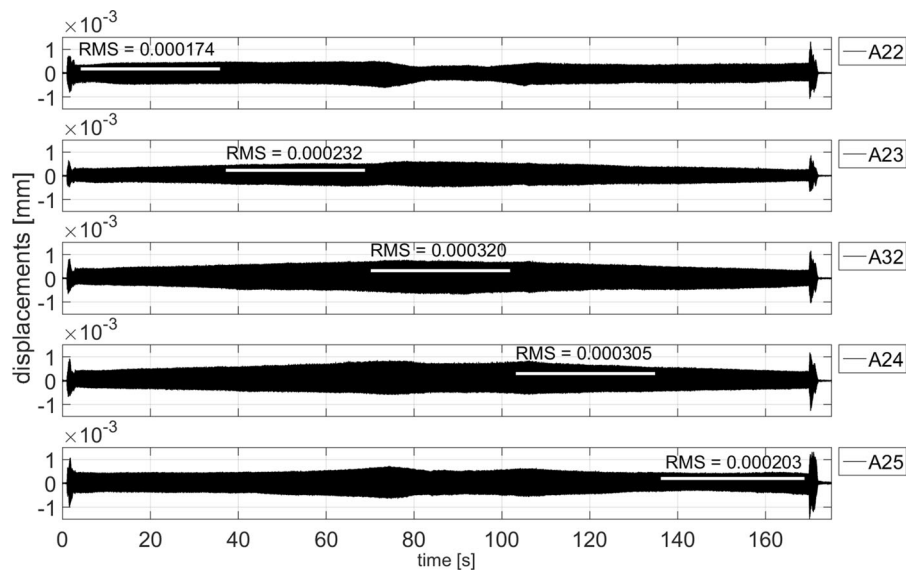Bold values indicate better results (i.e. greater RMS reduction)

interpreted as an indicator of the vibration level after correcting the surface displacement caused by tool deflection in the workpiece. This corresponds better to the way how vibrations are measured during the real milling process, because during acceleration measurements "static" components of the machined surface deflection are omitted.

The values of the abovementioned indices for simulated spindle speeds are presented in appropriate figures. According to the simulation results, spindle speed $n = 1380$ rev/min ($v_f = 637$ mm/min) was selected for surface 1 as the best (Fig. 4) and was applied for milling process. Two exemplary plots of simulation results are presented in Fig. 5. For surface 2 as the best spindle speed $n = 700$ rev/min ($v_f = 1541$ mm/min) was selected (Fig. 6) and applied for milling. Additionally, $n = 800$ rev/min was also applied for milling in order to present an alternative spindle speed, as it was shown by simulations.

Fig. 7 Vibrations of workpiece during full milling of surface 1 at standard parameters (see Table 2)

Fig. 8 Vibrations of workpiece during full milling of surface 1, modal approach (see Table 2)

Approximate simulation time in case of milling with single passes of both surfaces was about 30 min. Real milling results are presented and discussed in Sect. 4.4.

The suggested method results in a solution to improve milling (compare Figs. 4, 6). It allows to determine appropriate conditions at which the workpiece vibration level approaches minimum.

4.4 Real milling results

Milling operations were performed for both workpiece surfaces and various spindle speeds selected according to standard parameters and the abovementioned method. In the Table 2 selected spindle and feed speeds are presented. In Tables 2, 3 and 4 sign "Axx" denotes given accelerometer's number (see, Fig. 3b). In the Table 3, RMS values of displacements for

performed milling operations observed in measurement points during passing the tool over the given sensor, are presented. For example, value for sensor A22 was calculated for time period from the beginning of the milling operation (excluding the time period while the tool was entering into the material) to the instant of time when the tool was in the middle between positions of sensor A22 and A23 (see, Figs. 7, 8 for an illustrative example and Fig. 3b for sensors positions). Displacements values were calculated by double integration of the measured accelerations. Table 4 presents the same data but as the relative values. The latter helps to notice that the approach provides better results towards vibration suppression. Vibration reduction is denoted with the "−"sign. First, milling with the standard parameters was performed and its results are recognized as the reference for subsequent tests. The presented methods of the best spindle speed selection was examined. Chosen results of the measurement are shown (Figs. 7, 8).

The application of the modal approach to milling surface 1 allows EAVP to choose the best spindle speed for which the simulation results are overestimated in relation to the measured average displacements (Fig. 4, Table 3), and for surface 2—the results of down milling are somewhat underestimated (Fig. 6, Table 3). There is currently no explanation for this phenomenon. Most important, however, is that in reality this approach gave milling results better than standard types.

5 Conclusions

The efficiency of the proposed method of vibration suppression has been proven by selecting the best spindle speed when milling large-size structures using a dedicated technique of Experiment Aided Virtual Prototyping (EAVP). Thanks to the results of the modal approach, and thus—the identification of the modal subsystem obtained by the ERA method, it can be concluded that the parameters obtained from the experiment and provided from the calculation model were correctly determined and constitute reliable process data for simulation tests. This is confirmed by 9 natural frequencies identified for the spectrum band up to 500 Hz.

In general, the proposed method ensures and also allows to predict—satisfactory results of the reduction of tool and workpiece vibration, in some cases up to 50%, especially in the case of down milling operation. The advantage of the modal approach is the accuracy of the results of the computer prediction of the best spindle speed, which makes them attractive for practical applications in an industrial environment. However, creating a full FEM model in this approach means spending a lot of time both building the model and adapting it to the results of experimental modal tests. In the case of larger or more complex components, it can take many hours of labor, and thus—generate unnecessary economic follow-ups. Tests are limited to treated surfaces only. Nevertheless, reliable dynamic behavior of the machined surface will be identified when all modes affecting a particular surface are observed during this limited modal test.

Compliance with ethical standards

Conflict of interest The authors declare that they have no conflict of interest.

References

1. Ajayan M, Nishad PN (2014) Vibration control of 3D gantry crane with precise positioning in two dimensions. In: annual

international conference on IEEE emerging research areas: magnetics, machines and drives (AICERA/iCMMD), 24–26 July 2014, pp 1–5

2. Nouari M, List G, Girot F (2003) Wear mechanisms in dry machining of aluminium alloys. Int J Mech Prod Syst Eng 4:22–29

3. Quintana G, Ciurana J (2011) Chatter in machining processes: a review. Int J Mach Tools Manuf 51:363–376

4. Tomkow J (1997) Vibrostability of machine tools (in Polish). The Scientific and Technical Publication, Warsaw

5. Mané I, Gagnol V, Bouzgarrou BC, Ray P (2007) Stability-based spindle speed control during flexible workpiece high-speed milling. Int J Mach Tools Manuf 48:184–194

6. Munoa J, Beudaert X, Dombovari Z, Altintas Y, Budak E, Brecher C, Stepan G (2016) Chatter suppression techniques in metal cutting. CIRP Ann Manuf Technol 65:785–808

7. Kalinski KJ, Galewski MA (2015) Optimal spindle speed determination for vibration reduction during ball-end milling of flexible details. Int J Mach Tools Manuf 92:19–30

8. Kalinski KJ, Galewski MA, Mazur MR (2014) High speed milling vibration surveillance with optimal spindle speed based on optimal speeds map. Key Eng Mater 597:125–130

9. Kalinski KJ, Mazur MR, Galewski MA (2013) Optimal spindle speed map for chatter vibration reduction during milling of bow thruster blade. Solid State Phenom 198:686–691

10. Kalinski KJ, Galewski MA (2011) Chatter vibration surveillance by the optimal-linear spindle speed control. Mech Syst Signal Process 25(1):383–399

11. Soliman E, Ismail F (1997) Chatter suppression by adaptive speed modulation. Int J Mach Tools Manuf 37(3):355–369

12. Liao YS, Young YC (1996) A new on-line spindle speed regulation strategy for chatter control. Int J Mach Tools Manuf 35(6):651–660

13. Tarng YS, Lee EC (1997) A critical investigation of the phase shift between the inner and outer modulation for the control of machine tool chatter. Int J Mach Tools Manuf 37:1661–1672

14. Song Q, Ju G, Liu Z, Ai X (2014) Subdivision of chatter-free regions and optimal cutting parameters based on vibration frequencies for peripheral milling process. Int J Mech Sci 83:172–183

15. Ganguli A, Deraemaeker A, Preumont A (2007) Regenerative chatter reduction by active damping control. J Sound Vib 300:847–862

16. Naranjo W, Fajardo WJ, Motato E (2011) Active vibration control of gantry structures using PZT actuators. ASME 2:201–208

17. Monnin J, Kuster F, Wegener K (2014) Optimal control for chatter mitigation in milling—part 1: modeling and control design. Control Eng Pract 24:156–166

18. Rashid A, Nicolescu CM (2005) Active vibration control in palletised workholding system for milling. Int J Mach Tools Manuf 46(12–13):1626–1636

19. Munoa J, Beudaert X, Erkorkmaz K, Iglesias A, Barrios A, Zatarain M (2015) Active suppression of structural chatter vibrations using machine drives and accelerometers. CIRP An Manuf Technol 65:785–808

20. Moradi H, Vossoughi G, Behzad M, Movahhedy MR (2015) Vibration absorber design to suppress regenerative chatter in nonlinear milling process: application for machining of cantilever plates. Appl Math Model 39:600–620

21. Yang Y, Dai W, Liu Q (2014) Design and implementation of two-degree-of-freedom tuned mass damper in milling vibration mitigation. J Sound Vib 335:78–88

22. Hao Q, Guan L, Wang L, Shao H (2010) Dynamic feed-forward control of the 2-DOFs parallel manipulator of a hybrid machine tool. In: Proceedings of 8th IEEE international conference on control and automation, pp 528–533

23. Kalinski KJ (2012) A surveillance of dynamic processes in mechanical systems (in Polish). The Publication of Gdansk University of Technology, Gdansk

24. Chodnicki M, Kalinski KJ, Galewski MA (2013) Vibration surveillance during milling of flexible details with the use of active optimal control. J Low Frequency Noise Vib Active Control 32:145–156

25. Ding Y, Zhang XJ, Ding H (2015) Harmonic differential quadrature method for surface location error prediction and machining parameter optimization in milling. J Manuf Sci Eng 137:024501-1–024501-6

26. Cao G, Liu Y, Hu S (2010) Technology roadmap for technology innovation: a case of heavy-duty and large-size CNC machine tool industry in Hubei. In: 2010 international conference on management and service science, pp 1–4

27. Kaliński KJ, Galewski MA, Mazur M, Morawska N (2019) Optimization of the spindle speed during milling of large-sized structures with the use of technique of experiment-aided virtual prototyping. In: Awrejcewicz J, Kaźmierczak M, Olejnik P (eds) Applicable solutions in non-linear dynamical system. DSTA 2019. Lodz University of Technology, Lodz, pp 249–258

28. Kalinski KJ (1997) The finite element method application to linear closed loop steady system vibration analysis. Int J Mech Sci 39:315–330

29. Uriarte L, Zatarain M, Axinte D et al (2013) Machine tools for large parts. CIRP Ann Manuf Technol 62(2):731–750

30. Sarhan AD, Besharaty SR, Akbaria J, Hamdi M (2015) Improvement on a CNC gantry machine structure design for higher machining speed capability. World Academy of Science, Engineering and Technology. Int J Mech Aerosp Ind Mechatron Manuf Eng 9:534–538

31. Kaliński KJ, Galewski MA, Mazur M, Chodnicki M (2017) Modelling and simulation of a new variable stiffness holder for milling of flexible details. Polish Marit Res 24:115–124

32. Allemang RJ (2003) The modal assurance criterion—twenty years of use and abuse. Sound Vib 37:14–21

33. Galewski MA (2017) Application of the labview environment for experimental modal analysis support (in Polish). In: Kaliński KJ, Lipiński K (eds) From finite element method to mechatronics. The Publication of Gdansk University of Technology, Gdansk, pp 105–118

34. Totis G, Albertelli P, Torta M, Sortino M, Monno M (2017) Upgraded stability analysis of milling operations by means of advanced modeling of tooling system bending. Int J Mach Tools Manuf 113:19–34

35. Maia NMM, Silva JMM (1997) Theoretical and experimental modal analysis. Research Studies Press, Taunton

Springer